Available online at www.sciencedirect.com
SCIENCE DIRECT®
Journal of Catalysis 227 (2004) 227–241
JOURNAL OF CATALYSIS
www.elsevier.com/locate/jcat

Xylene isomerization and aromatic alkylation in zeolites NU-87, SSZ-33, β, and ZSM-5: molecular dynamics and catalytic studies

Francisco J. Llopis [a,b], German Sastre [a], Avelino Corma [a,*]

[a] *Instituto de Tecnologia Quimica, UPV-CSIC, Av/Naranjos s/n, 46022 Valencia, Spain*
[b] *Departamento de Ingenieria Quimica, UVEG, Universitat de València, C/Dr. Moliner 50, 46100 Burjassot, Valencia, Spain*

Received 15 April 2004; revised 5 July 2004; accepted 9 July 2004

Abstract

The unique pore topology of zeolite NU-87, with 10-membered ring (MR) channels intersected by perpendicular 12-MR cavities, can offer new opportunities for alkylaromatics isomerization, as well as for aromatics alkylation. The catalytic performance has been studied for *meta*-xylene isomerization and disproportionation, as well as toluene alkylation with methanol, ethanol, propanol, and isopropanol. Product distribution was interpreted on the basis of pore topology and compared to zeolites with 12-MR (β), 10- and 12-MR (SSZ-33), and 10-MR (ZSM-5) zeolites. The presence of cavities allows more space for the location of bulky intermediates and/or products, and also traps the molecules, allowing consecutive reactions that lead to thermodynamic equilibrium. Channels, on the other hand, allow diffusion without trapping, if their free diameter is large enough. 10-MR channels in NU-87 are smaller than in ZSM-5 and this limits diffusivity. Furthermore, trimethylbenzenes formed will tend to equilibrate, but only the smaller isomer, i.e., 1,2,4-trimethylbenzene, fits in the NU-87 cavity and will have a small chance to diffuse. Catalytic experiments as well as atomistic molecular dynamics are used to interpret the behavior of NU-87 and to explain the results in comparison with other structures.
© 2004 Elsevier Inc. All rights reserved.

Keywords: Reactivity NU-87 zeolite; Reactivity SSZ-33 zeolite; Aromatics alkylation with zeolites; Cumene production with zeolites; Xylene isomerization with 10 and 12MR zeolites; Diffusion of aromatics in zeolites

1. Introduction

Zeolites with connected channels of 10 and 12 MR (membered rings) offer an interesting pore arrangement for catalysis, since they may combine high conversion and shape-selectivity features [1,2]. Large channels of 12 MR allow large molecules to diffuse and react, while products formed may diffuse with different abilities in the two pore systems available [3]. Preferential diffusion paths may exist depending on the relative size of the reactants and products. This was shown (by molecular dynamics simulations) to be the case for the diffusion of *ortho* and *para*-xylene in a CIT-1 structure with crossing channels of 10 and 12 MR, where relative *para*/*ortho*-xylene diffusivities of 3.2 and 2.3 were found at low and high loading, respectively [4]. A different situation appears in MCM-22 [5] with a sinusoidal 10-MR channel and a separated set of 12-MR cavities connected by 10-MR openings. In this case the two channel systems are independent and their relative contribution to the catalytic behavior for different reactions depends on the reactant size [6]. The relative contribution of the two-channel systems can also be tuned by delaminating a laminar precursor [7] of the MCM-22, thus increasing the external surface while preserving the 10-MR channels [8]. By doing this, the accessibility of larger molecules to the active centers is increased and the combined benefits of both pore systems was improved from the point of view of acidity and catalytic activity for particular reactions [9].

NU-87 contains 12-MR cages with four 10-MR entrances forming channels [10] as shown in Fig. 1. A number of patents have come out in the last few years that show potential catalytic applications [11,12]. It is clear that the catalytic

* Corresponding author.
E-mail address: acorma@itq/upv.es (A. Corma).

0021-9517/$ – see front matter © 2004 Elsevier Inc. All rights reserved.
doi:10.1016/j.jcat.2004.07.014

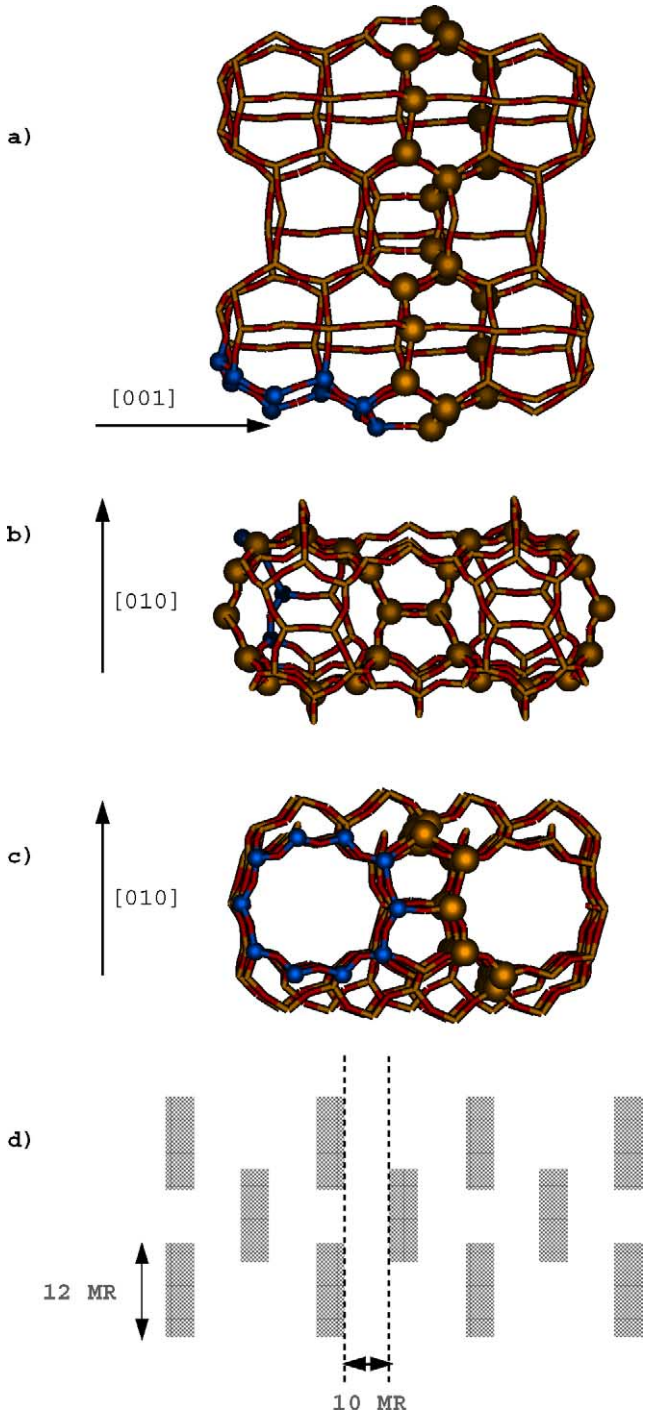

Fig. 1. Three views of two consecutive cavities of NU-87 zeolite (where 12 MR are shown in large ball sticks and 10 MR are shown in small ball sticks) showing the shape of the cage and their relative orientation (a); the 12 MR that form the cross section of the cavity (b); the 10 MR forming the channels connecting cavities (c); and a scheme of the microporous network (d).

behavior of such zeolite should be related to its particular pore topology of 10 and 12 MR forming a unique arrangement. We have tried to rationalize the relationship between pore topology of NU-87 and its catalytic properties by combining computer simulation and catalytic experiments. Some C8 and C9 aromatics have been simulated through atomistic molecular dynamics which allow calculation of the self-diffusivity. On the other hand, experiments are performed for C8 *meta*-xylene isomerization and disproportionation as well as toluene alkylation with methanol, ethanol, and isopropanol. The results are explained in terms of diffusion and transition-state shape selectivity and, in order to provide further and more solid conclusions, the study has been extended to other zeolites, with 12-MR channels (β), 10- and 12-MR channels (SSZ-33), and 10-MR channels (ZSM-5).

2. Methodology

2.1. Molecular dynamics technique

Atomistic molecular dynamics (md) calculations have been performed to simulate the diffusion of *ortho*-xylene, *para*-xylene, and 1,2,4-trimethylbenzene (TMB) in purely siliceous NU-87, β, SSZ-33, and ZSM-5. The calculations require the specification of a potential energy function which provides a description of the energy of the system as a function of nuclear coordinates and allows the calculation of its first derivatives from which the forces acting on each atom can be obtained. All the md simulations have been carried out using the general purpose DL_POLY_2.13 code [13], developed to run on a wide variety of computer architectures, including workstations and massive parallel platforms. Our current implementation was optimized for running in a SGI Origin 3800 using 16 processors. The parallel version is written in the replicated data form and uses MPI (message passing interface), a standard message passing system of libraries, as well as highly optimized hardware-specific communications.

The simulation proceeds by first assigning initial velocities to all atoms according to a Maxwell–Boltzmann distribution which depends on the temperature of the system. From this starting point, Newton's equations of motion are solved using a finite time step by means of the standard Verlet algorithm [14]. Time steps of 1 fs and an equilibration temperature of 650 K have been employed in the present simulations. The pure silica zeolitic systems comprise 2448, 1536, 1344, and 1152 atoms for NU-87, β, SSZ-33, and ZSM-5, respectively, to which parallelepiped periodic boundary conditions are applied. A unique loading of aromatics in each system is modeled (14 molecules in NU-87, 11 molecules in β, 16 molecules in SSZ-33, and 10 molecules in ZSM-5) with the same periodic boundary conditions applied to the sorbates in the zeolite. The geometry of the zeolite is first optimized at 0 K using the BFGS [15] technique implemented in the GULP [16] code, and the result is used as input for a 50 ps equilibration stage of the zeolite + sorbate system. A "cap forces" directive (limited to 1000 kT/Å) avoids the collision between the atoms of the system during the initialization. After the initialization period, the velocity rescaling algorithm is removed and a run of 10 ps is performed to ensure that the temperature remains constant at 650 K within a

fluctuation of ±5 K. After this period, runs of 500 ps were carried out within the NVE ensemble at 650 K. Three simulations, one with each pure sorbate (*ortho*-xylene, *para*-xylene, and 1,2,4-trimethylbenzene), were considered.

Full motion of the framework atoms has been considered throughout the simulations. Although this increases substantially the computational expense, the influence of the framework flexibility has been made clear in a number of studies [17–19]. During the simulation, history files were saved every 100 steps, and subsequent analysis used the MSD facility included in DL_POLY to obtain mean-square displacements. The expression used to calculate the MSD plots was the following [20],

$$\left\langle X^2(t)\right\rangle = 1/(N_{\mathrm{m}}N_{\mathrm{to}})\sum_i\sum_{t_0}\left[X_i(t+t_0)-X_i(t_0)\right]^2, \qquad (1)$$

where N_{m} is the number of diffusing molecules, N_{to} is the number of time origins used in calculating the average, and X_i is the coordinate of the center of mass of molecule i.

The diffusion coefficients are then calculated from the Einstein relation,

$$\left\langle X^2(t)\right\rangle = 6Dt + B, \qquad (2)$$

where t is the simulation time, and B is the thermal factor arising from atomic vibrations.

2.2. Interatomic potentials

Four types of interatomic potentials are needed to model this system:

$$V_{\mathrm{total}} = V_{\mathrm{zeolite}} + V_{\mathrm{organic}} + V_{\mathrm{organic\text{–}organic}} + V_{\mathrm{zeolite\text{–}organic}}. \qquad (3)$$

The potential for the framework, V_{zeolite}, was originally derived by Catlow et al. [21], and is essentially a Born model potential comprising three terms:

$$V_{\mathrm{zeolite}} = V_{\mathrm{buck}} + V_{\mathrm{three\text{-}body}} + V_{\mathrm{Coul}}. \qquad (4)$$

The first is a short-range, polynomial, four-range Buckingham splined function (see Table 1) for which a cutoff distance of 7.6 Å was used. A three-body, O–Si–O, nonharmonic potential was chosen to describe bond-angle-bending forces. Finally, the long-range electrostatic interactions were calculated by means of the Ewald summation technique using formal charges.

The potential for the sorbate, V_{organic}, comprises four terms and was taken from Oie et al. [22]:

$$V_{\mathrm{organic}} = V_{\mathrm{two\text{-}body}} + V_{\mathrm{three\text{-}body}} + V_{\mathrm{four\text{-}body}} + V_{\mathrm{Coul}}. \qquad (5)$$

Four different atom types are considered in the xylene molecule: CA, CB, HA, and HB, the atoms marked A belonging to the aromatic ring, and those marked B forming part of the methyl groups. The potential includes harmonic two-body and three-body bond-bending terms for the interactions CA–CA, CA–CB, HA–CA, HB–CB; and CA–CA–CA, CA–CA–CB, HB–CA–CB, HA–CA–CA, and HB–CB–HB. The four–body interaction is described by a cosine potential (see Table 2) for the quartets, CA–CA–CA–CA, CA–CA–CA–CB, HB–CB–CA–CA, HA–CA–CA–CB, HA–CA–CA–CA, and HA–CA–CA–HA. A total of 18 bond terms, 30 angle terms, and 36 dihedral-angle terms are employed to describe the aromatic molecules. Partial charges of −0.153 and +0.483 for CA and CB, respectively, and +0.153 and −0.11 for HA and HB, respectively, were used for the coulombic interactions in the fourth term of Eq. (5) and were taken from Auerbach et al. [23]. All the parameters used are given in Table 2.

Table 1
Potential form for the all silica zeolites

$V_{\mathrm{zeolite}} = V_{\mathrm{buck}} + V_{\mathrm{three\text{-}body}} + V_{\mathrm{Coul}}$ [Eq. (4)][a]

$V_{\mathrm{buck}} = A_{ij}\exp(-r_{ij}/\rho_{ij}), \quad r_{ij} < r_1$

$V_{\mathrm{buck}} = B_{ij}(r_{ij})^5 + C_{ij}(r_{ij})^4 + D_{ij}(r_{ij})^3 + E_{ij}(r_{ij})^2 + F_{ij}r_{ij} + G_{ij}, \quad r_1 < r_{ij} < r_2$

$V_{\mathrm{buck}} = H_{ij}(r_{ij})^3 + I_{ij}(r_{ij})^2 + J_{ij}r_{ij} + K_{ij}, \quad r_2 < r_{ij} < r_3$

$V_{\mathrm{buck}} = -L_{ij}/(r_{ij})^6, \quad r_3 < r_{ij} < r_c$

$V_{\mathrm{three\text{-}body}} = (1/4)A_{ijk}(B_{ijk})^2\exp(-r_{ij}/\lambda)\exp(-r_{ik}/\lambda)$, where $A_{ijk} = (1/2)K_{ijk}(\theta_0-\pi)^{-2}$, $B_{ijk} = (\theta_0-\pi)^2 - (\theta-\pi)^2$

$V_{\mathrm{Coul}} = q_j\cdot q_j/r_{ij}$, where $q(\mathrm{O}) = -2.0$, $q(\mathrm{Si}) = +4.0$

Parameter	Si–O	O–O
r_1 (Å)	1.5	2.9
r_2 (Å)	2.5	3.6
r_3 (Å)	3.5	4.2
r_c (Å)	7.6	7.6

[a] The short-range Buckingham potential for Si–O and O–O interactions is a function splined at r_1, r_2, and r_3 to have continuous first and second derivatives, and a minimum at r_2. A cutoff distance $r_{\mathrm{c}} = 7.4$ Å was employed in the md simulations.

Finally, 12-6 Lennard–Jones potentials and coulombic interactions (with the charges already noted) were used to describe the guest–guest and framework–guest interactions according to the following equations:

$$V_{\mathrm{organic\text{–}organic}} = V_{\mathrm{Lennard\text{–}Jones}} + V_{\mathrm{Coul}}, \qquad (6)$$

$$V_{\mathrm{zeolite\text{–}organic}} = V_{\mathrm{Lennard\text{–}Jones}} + V_{\mathrm{Coul}}. \qquad (7)$$

The guest–guest terms included were CA–CA, CA–CB, CB–CB, CA–HA, CA–HB, CB–HA, CB–HB, HA–HA, HA–HB, and HB–HB. As for framework–guest interactions, the terms included were CA–SI, CB–SI, HA–SI, HB–SI, CA–O, CB–O, HA–O, and HB–O. These parameters are listed in Table 3 and were taken from Ref. [21] in which the guest molecule considered is benzene. In the $V_{\mathrm{organic\text{–}organic}}$ and $V_{\mathrm{zeolite\text{–}organic}}$ potentials, additional terms must be included in the summation to take into account interactions due to the substituent methyl groups in the aromatic ring.

Table 2
Potential form and parameters used for *ortho*- and *para*-xylene and 1,2,4-trimethylbenzene molecules

$V_{\text{xylene}} = V_{\text{two–body}} + V_{\text{three-body}} + V_{\text{four-body}} + V_{\text{Coul}}$ [Eq. (5)]

$V_{\text{two-body}} = (1/2)k_{ij}(r_{ij} - r_{ij}^0)^2$

$V_{\text{three–body}} = (1/2)k_{ijk}(\theta_{ijk} - \theta_{ijk}^0)^2$

$V_{\text{four-body}} = A_{ijkl}[1 + \cos(n\phi_{ijk} - \delta_{ijkl})]$

$V_{\text{Coul}} = q_j q_j / r_{ij}$,

where $q(\text{CA}) = -0.153$, $q(\text{CB}) = +0.483$, $q(\text{HA}) = +0.153$, $q(\text{HB}) = -0.110$

Two-body parameters	k_{ij} (eVÅ^{-2})	r_{ij}^0 (Å)
CA–CA	48.94	1.385
CA–CB	31.75	1.510
CA–HA	31.25	1.085
CB–HB	28.75	1.095

Three-body parameters	k_{ijk} (eV)	θ_{ijk}^0 (°)
CA–CA–CA	3.44	120.0
CA–CA–CB	3.44	120.0
CA–CA–HA	3.44	120.0
CA–CB–HB	2.50	109.5
HB–CB–HB	2.06	109.5

Four-body parameters	A_{ijkl} (eV)	n	δ_{ijkl} (°)
CA–CA–CA–CA	0.2166	2.0	180.0
CA–CA–CA–HA	0.0867	2.0	180.0
CA–CA–CA–CB	0.0867	2.0	180.0
CB–CA–CA–HA	0.0867	2.0	180.0
HA–CA–CA–HA	0.0867	2.0	180.0
CA–CA–CB–HB	0.0043	3.0	0.0

2.3. Structural data

NU-87 [10], whose International Zeolite Association code is NES [24], is a zeolite containing channel systems with 10 and 12 MR. The 12 MR are parallel to [001] and form the cross section of a large cavity whose cross section is formed by 12 MR of dimensions 5.3 × 6.8 Å. Perpendicularly to these windows, across [101], a 10-MR channel system appears, with dimensions 5.7 × 4.8 Å. A view of the cavities and channels is provided in Fig. 1. β zeolite [25], with code BEA [24], has two connected 12-MR channel systems with dimensions 6.6 × 6.7 Å (parallel to [100] and [010]) and 5.6 × 5.6 Å (parallel to [001]). ZSM-5 [26], with code MFI [24], contains interconnected channels of 10-MR parallel to [100] (5.1 × 5.5 Å) and to [010] (5.3 × 5.6 Å). Finally, SSZ-33 [27] is an intergrowth of two polymorphs (A and B) with a predominance of polymorph B, with code CON [24], and a fault probability close to 30%, and it contains 12- and 10-MR interconnected channels of 6.4 × 7.0 Å, 5.9 × 7.0 Å (12 MR parallel to [001] and [100], respectively), and 4.5 × 5.1 Å (10 MR parallel to [010]).

In this part of the study we make extensive use of visualization of trajectories of the sorbate molecules center of mass, in order to elucidate the diffusion process in the different channel systems. The md simulations give, as output, a history file with the Cartesian coordinates of all the atoms of the system as a function of time. In order to visualize the history files, we generate *trajectory graphs* corresponding to x vs y and x vs z in order to visualize the diffusion path, where x, y, z correspond in each case to the crystallographic axes. Instead of superimposing the channels in the drawing we have left only the trajectories, and from them the channel location can be easily guessed.

Table 3
Potential parameters used for xylene–xylene and zeolite–xylene interactions

$V_{\text{organic–organic}} = V_{\text{Lennard–Jones}} + V_{\text{Coul}}$ [Eq. (6)]

$V_{\text{zeolite–organic}} = V_{\text{Lennard–Jones}} + V_{\text{Coul}}$ [Eq. (7)]

$V_{\text{organic–organic}} = (A_{ij}/r_{ij})^{12} - (B_{ij}/r_{ij})^6$

$V_{\text{zeolite–organic}} = (A_{ij}/r_{ij})^{12} - (B_{ij}/r_{ij})^6$

Lennard–Jones parameters	A_{ij} (eV Å^{12})	B_{ij} (eV Å^6)
CA–CA	32475.0	29.838
CA–CB	32475.0	29.838
CB–CB	19692.0	18.0933
CA–HA	3721.2	7.6182
CA–HB	3721.2	7.6182
CB–HA	2800.0	5.8415
CB–HB	2800.0	5.8415
HA–HA	384.840	1.9867
HA–HB	384.840	1.9867
HB–HB	384.840	1.9867
CA–O	15000.0	22.402
CB–O	11000.0	17.654
HA–O	1556.4	5.5717
HB–O	1556.4	5.5717

Table 4
Characteristics of samples used in this work

Sample	ZSM-5	NU-87	SSZ-33	Beta
Si/Al ratio	20	17	20	13
Crystal size (μm)	0.1	0.3–0.4	1	0.17
S (BET) (m^2/g)	379	390	500	457
Pore volume (cm^3/g)	0.15	0.17	0.21	0.25
Brönsted acidity (μmol Py/g)				
$T = 523$ K	66.4	71.3	53.1	32.9
$T = 623$ K	52.2	54.7	47.6	27.4
$T = 673$ K	30.8	40.4	33.3	5.5
Lewis acidity (μmol Py/g)				
$T = 523$ K	47.4	10.8	20.7	31.1
$T = 623$ K	36.7	7.2	19.3	25.1
$T = 673$ K	24.5	10.8	14.4	21.0

Crystal size estimated from SEM pictures. Acid strength distribution determined by IR-pyridine measurements at different desorption temperatures, using the extinction coefficients given by Emeis [56].

3. Experimental materials

Zeolites NU-87 [11] and SSZ-33 [28] have been synthesized following the procedures reported in the literature and their characteristics are given in Table 4. ZSM-5 sample

(CBV 5020) was provided by PQ Corporation, and zeolite β was prepared in our laboratory. Si/Al ratios were determined by chemical analysis.

No ion exchange was performed. The acid zeolites were obtained by direct calcination of the organic forms at 853 K for 3 h under air flow before use. The porosity was determined by nitrogen adsorption at 77 K, and the acidic properties were characterized by infrared and pyridine adsorption followed by desorption at 523, 623, and 673 K. Surface-area measurements were obtained by the standard BET method. The average crystallite size of the zeolites was determined by scanning electron microscopy (SEM) and the characteristics of all samples are given in Table 4.

4. Reaction procedure

Catalytic experiments were conducted in the vapor phase at atmospheric pressure in a fixed-bed continuous glass down-flow reactor (11 mm internal diameter). The catalyst (with particle size within the range 0.3–0.5 mm) was diluted with glass in order to maintain a constant bed volume.

The *meta*-xylene isomerization was carried out with *meta*-xylene/N_2 molar ratio of 0.25. For alkylation reactions toluene was fed in excess of alcohol in a molar ratio of 4. N_2 was used as a gas carrier in a N_2 to alcohol molar ratio of 1/1. Prior to the addition of reactants, the catalyst was heated at 623 K at a heating rate of 5 K/min, under a flow of nitrogen. After 30 min, the temperature was raised to 723 K and kept at that temperature for 1 h. The reactor was then cooled down to reaction temperature, 623 K for *meta*-xylene isomerization or 573 K for toluene alkylation. When the temperature was stabilized, the reactants were fed at the top of the reactor. The reactor exit was connected to a multisampling controlled heated valve equipped with six loops. The loops were automatically filled at preprogrammed times on stream (10, 30, 60, 180, and 360 s). The products of the reaction were analyzed subsequently in a gas chromatograph (HP5890II) equipped with a Supelco-WAX10 capillary column (60 m length, inner diameter 0.2 mm) and a flame ionization detector (FID).

Preliminary experiments were done in order to establish the conditions for which no control by external or internal diffusion exists. As the catalytic activity of the different zeolites differed substantially, the amount of catalyst in the reactor and the molar flow of reactants were adapted to obtain the desired degree of conversion. Initial selectivities were obtained from the initial rates of formation of the products. Initial conversions, X_0, and yields were calculated by extrapolating the conversion X, measured at different times on stream (t) according to the following equation:

$$X = X_0 \exp\left(-kt^{1/2}\right). \tag{8}$$

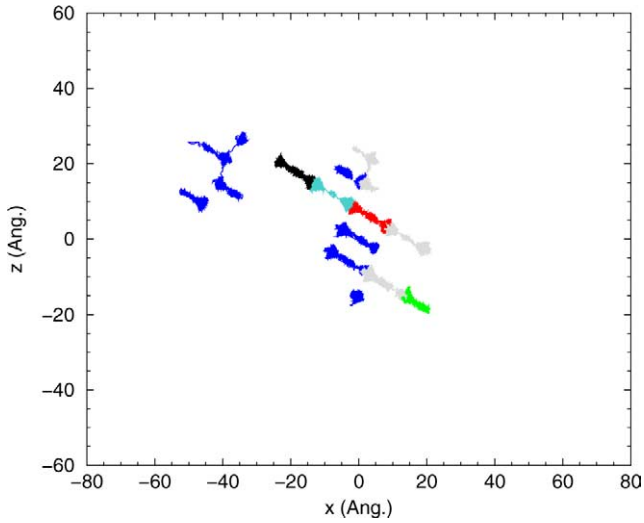

Fig. 2. Trajectory followed by 14 *ortho*-xylene molecules diffusing in NU-87 zeolite. Occasional intercage migration appears but it is only in rare events. Diffusivity is mainly intracavity and this happens with motions going from one side to the other in the cavity.

5. Molecular dynamics simulations

5.1. Diffusion in NU-87 (NES)

The diffusion path followed by *ortho*-xylene in NU-87 is shown in Fig. 2. It can be seen there that most of the molecules remain in the same cavity throughout the 500 ps simulation, indicating that intercavity diffusion is restricted due to the geometric impediment to leave the cavity through any of the four openings. Three such intercage events are observed in Fig. 2, but most events correspond to intracage diffusion. A large *intracavity mobility* is observed, this indicating that *ortho*-xylene molecules tend to locate not only at the minimum energy positions within the cavity but they can also cross from one side to the other within a given cavity. A very few cases are observed where the molecule remains at the same minimun position in the cavity, for example, the molecule located around the $(x, z) = (0, -15)$ in Fig. 2. A similar picture appears from Fig. 3 with respect to 1,2,4-trimethylbenzene. Although the size of this molecule is larger than that of *ortho*-xylene, and one may think that increasing branching may further complicate the diffusional ability, the trajectories found (Fig. 3) show very similar features. Only one migration from cage to cage is now observed at about $(x, z) = (-60, 10)$, and certainly less intracage mobility which leads to more extensive motions around the minimum energy position in the cavity. Paths with no intracage events, such as the one around $(x, z) = (-40, 10)$, are now more frequent than with *ortho*-xylene. *Para*-xylene (Fig. 4) behaves very differently regarding diffusion in the 10-MR channel system, and many intercage events are registered. Intracage events are also easily undertaken, as in *ortho*-xylene, and they are much more frequent than intercage events. It must be kept in mind that although 10 MR in NU-87 (5.7 × 4.8 Å) are suitable for diffusion of *para*-

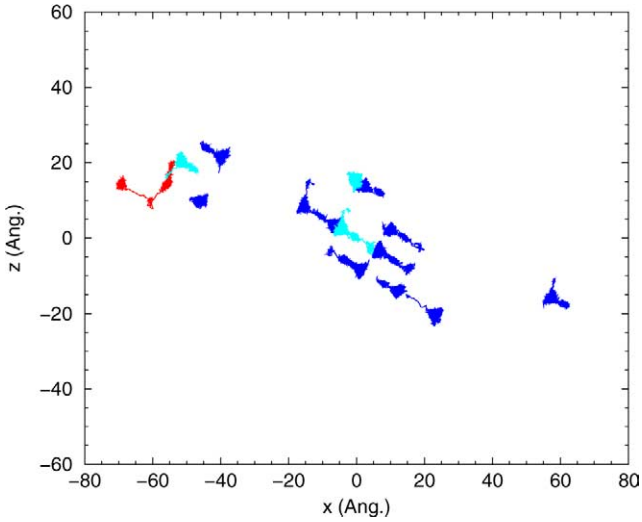

Fig. 3. Trajectory followed by 14 1,2,4-trimethylbenzene molecules diffusing in NU-87 zeolite. Intercage migration does appear but it is only in rare events. Diffusivity is mainly intracavity and this happens with motions going from one side to the other in the cavity, although the number of intracage motions is less frequent than with *ortho*-xylene.

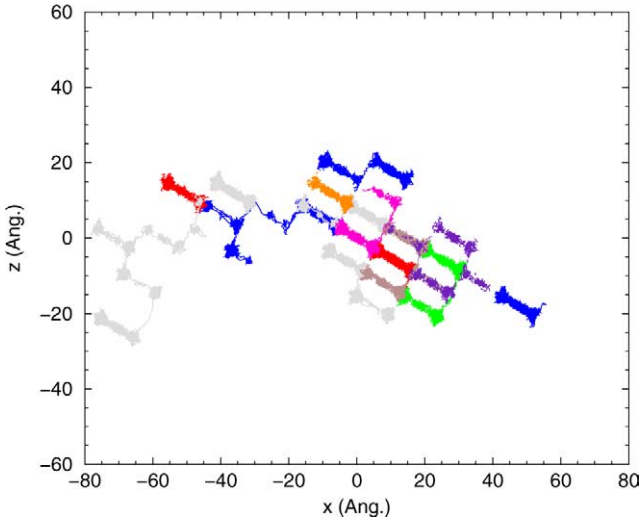

Fig. 4. Trajectory followed by 14 *para*-xylene molecules diffusing in NU-87 zeolite. Intercage migration is very frequent and also intracage motions contribute to the diffusivity. Trajectories of nearby molecules have been painted in different colors for better visualization.

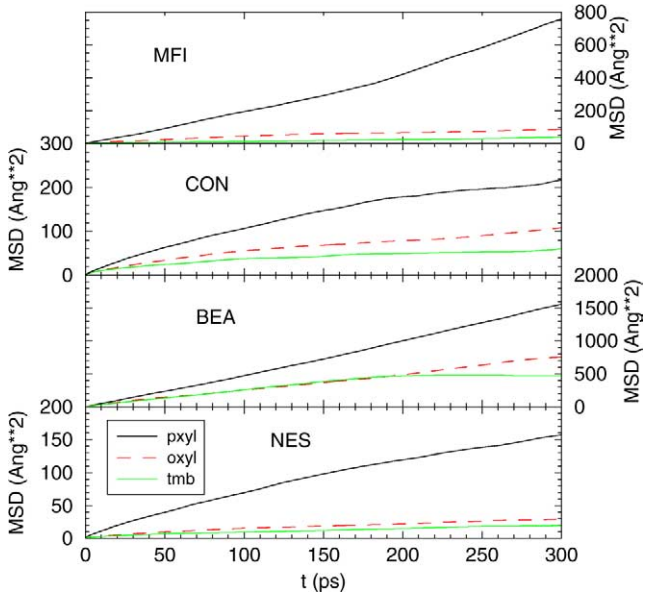

Fig. 5. Mean-square displacements from the molecular dynamics simulations for β with *ortho*- and *para*-xylene (top), and for NU-87 with *ortho*, *para*-xylene, and 1,2,4-trimethylbenzene (bottom). The diffusion coefficients obtained from these graphs are shown in Table 5.

Table 5
Diffusion coefficients from molecular dynamics simulations at 650 K

Sorbate in zeolite	Loading[a]	Diffusion coefficient[b]
ortho-Xylene in NU-87	0.017	1.42
para-Xylene in NU-87	0.017	8.30
1,2,4-Trimethylbenzene in NU-87	0.017	0.95
ortho-Xylene in β	0.021	28.31
para-Xylene in β	0.021	65.28
1,2,4-Trimethylbenzene in β	0.021	18.44
ortho-Xylene in ZSM-5	0.026	5.54
para-Xylene in ZSM-5	0.026	40.76
1,2,4-Trimethylbenzene in ZSM-5	0.026	1.81
ortho-Xylene in SSZ-33[c]	0.04	3.56
ortho-Xylene in SSZ-33[c]	0.01	7.79
para-Xylene in SSZ-33[c]	0.01	25.18
ortho-Xylene in SSZ-33	0.036	4.99
para-Xylene in SSZ-33	0.036	11.36
1,2,4-Trimethylbenzene in SSZ-33	0.036	2.53

[a] Organic molecules per SiO_2.
[b] (10–6 cm^2/s).
[c] From Ref. [4]. The simulated temperature is 500 K.

xylene, these 10-MR channels are smaller than other 10-MR systems, for example, ZSM-5 (5.5 × 5.1 and 5.6 × 5.3 Å). Besides the smaller diameter (at least in one dimension) of the 10-MR pore in NU-87, it should also be taken into account when discussing molecular diffusion that the 10-MR windows are not perpendicular to the channel direction (see Fig. 1a), and this further reduces the channel cross section.

In conclusion, the diffusion studies predict that while the three molecules can diffuse from one large cavity to another through the 10-MR channels of NU-87, the diffusion coefficients (see Fig. 5 and Table 5) should be lower than in a bidimensional 10-MR pore zeolite such as ZSM-5 and follow the order *para*-xylene > *ortho*-xylene > 1,2,4-trimethylbenzene. This, in turn, means that during *meta*-xylene isomerization, one can expect that reactants and products formed by methyl-shift isomerization or alkyl-shift transalkylation will spend a considerable time within the cavity before intercavity migration will occur. This should drive the mixture toward thermodynamic equilibrium, neutralizing diffusion shape-selectivity effects that will tend to enrich the gaseous stream with *para*-xylene. Furthermore, trimethylbenzenes formed will tend to equilibrate, and only the smaller isomer, i.e., 1,2,4-trimethylbenzene will have a small chance to diffuse. This effect should produce a high

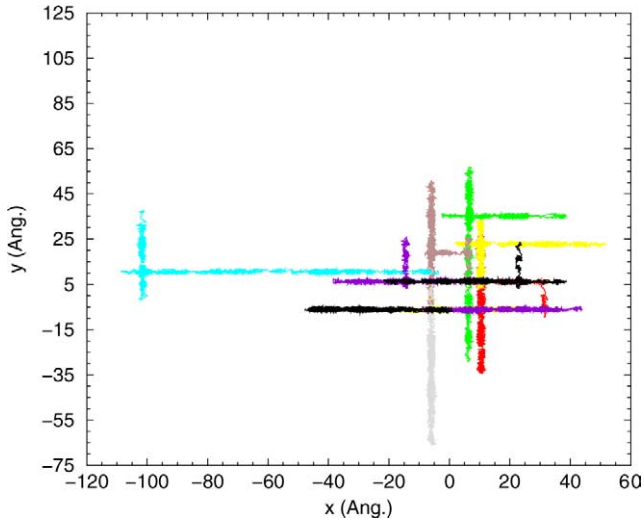

Fig. 6. Trajectory followed by 11 *ortho*-xylene molecules diffusing in β zeolite. Diffusion is not impeded by the larger channel size with respect to NU-87 where cavities and 10 MR are not present here.

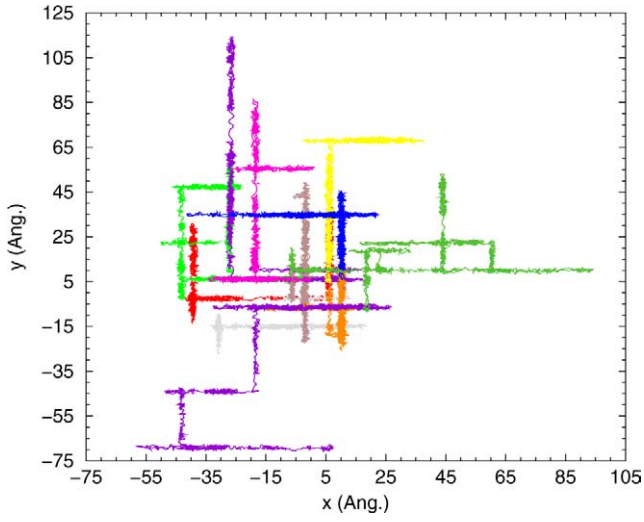

Fig. 7. Trajectory followed by 11 *para*-xylene molecules diffusing in β zeolite. Diffusion is larger than in the previous case (see Fig. 6) as shown by the larger trajectories drawn by the molecules. Trajectories of nearby molecules have been painted in different colors for better visualization.

selectivity to 1,2,4-trimethylbenzene, and a fast deactivation by pore blocking.

5.2. Diffusion in β (BEA)

A comparison with diffusivity of *ortho*- (Fig. 6) and *para*-xylene (Fig. 7) in β zeolite shows, as expected, that 12-MR channels (instead of cavities) and connections between channels allow a higher loading and faster diffusivity of the two isomers. Thus, a 12-MR channel system is much more suitable for diffusion than a system of 12-MR cavities interconnected through 10-MR channels, and this is not only because of the 10-MR intercage connection between cavities, but also due to the fact that changing the diffusion direction when entering and leaving the cavities makes a substantial drop in the diffusivity. Channels offer a less restricted trajectory system than cavities interconnected perpendicularly. This is shown by the much larger diffusion paths shown in Figs. 6 and 7, and also by the larger diffusion coefficients (Table 5) obtained from the mean-square displacements (Fig. 4). The diffusion of 1,2,4-trimethylbenzene (Fig. 8) is quite similar to *ortho*-xylene (Fig. 6), although shorter paths are observed in the former, which means that although the size of the 1,2,4-trimethylbenzene is suitable for diffusion in 12-MR channels, its larger size makes the diffusion more difficult.

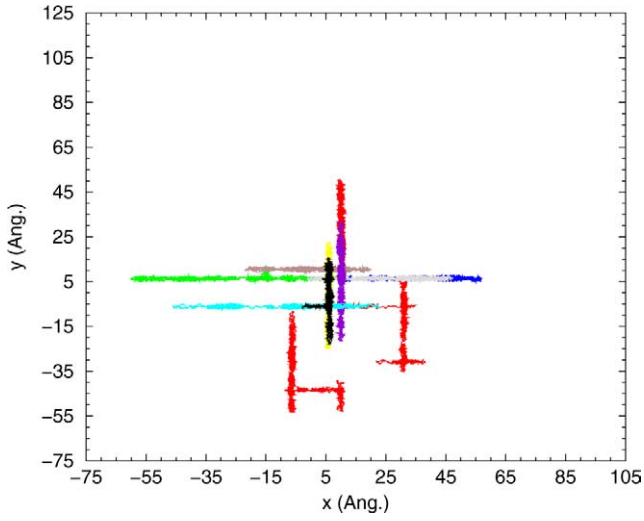

Fig. 8. Trajectory followed by 11 1,2,4-trimethylbenzene molecules diffusing in β zeolite. Diffusion is shorter than in the previous case (*para*-xylene) and similar to *ortho*-xylene (Fig. 6). Trajectories of nearby molecules have been painted in different colors for better visualization.

5.3. Diffusion in ZSM-5 (MFI)

This structure with only 10-MR channels shows very different diffusivities for *ortho*-xylene (Fig. 9) and *para*-xylene (Fig. 10) as can also be seen from the respective diffusion coefficients given in Table 5. In ZSM-5 the *para*/*ortho* ratio in the diffusion coefficients is 7.4, which is higher than that for NU-87. However, what is specially noticeable is the much larger diffusion coefficients for *para*- and *ortho*-xylene in ZSM-5, whereas that of 1,2,4-trimethylbenzene is much closer for both structures NU-87 and ZSM-5. These results would predict larger product diffusion shape-selectivity effects with ZSM-5. Finally, the diffusion of 1,2,4-trimethylbenzene (Fig. 11) is still slower than *ortho*-xylene as can be seen from the respective diffusion coefficient in Table 5. The larger size and the sinusoidal channel in ZSM-5 are responsible for the slower diffusivity observed in the case of 1,2,4-trimethylbenzene.

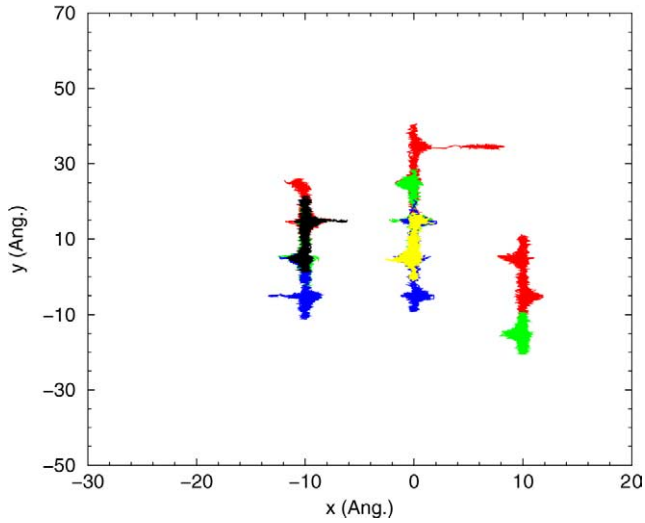

Fig. 9. Trajectory followed by 10 *ortho*-xylene molecules diffusing in ZSM-5 zeolite. Diffusion is strongly limited by the 10-MR channels.

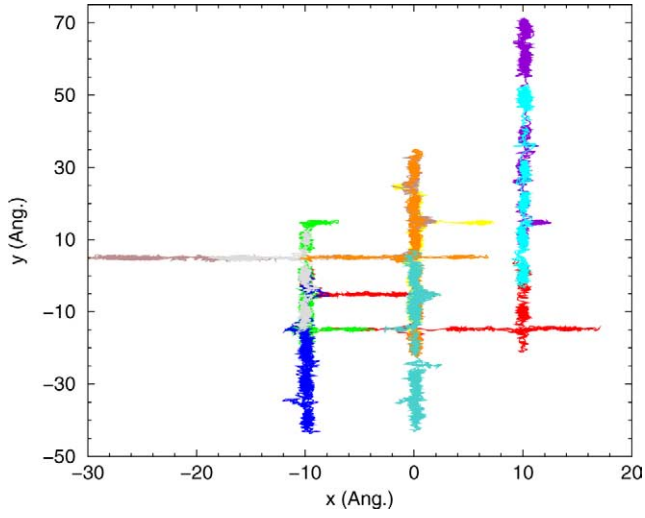

Fig. 10. Trajectory followed by 10 *para*-xylene molecules diffusing in ZSM-5 zeolite. Diffusion is enhanced by the close matching between the 10-MR channels and the *para*-xylene sizes.

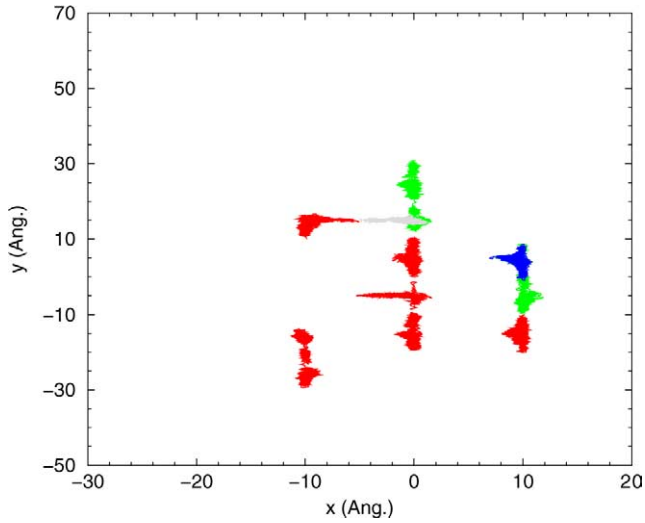

Fig. 11. Trajectory followed by 10 1.2.4-trimethylbenzene molecules diffusing in ZSM-5 zeolite. Diffusion is strongly limited by the 10-MR channels, even more than in the case of *ortho*-xylene (Fig. 9).

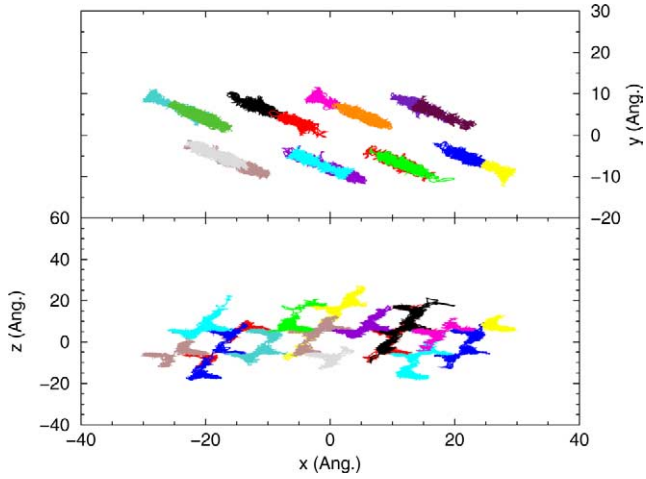

Fig. 12. Trajectories followed by 16 *ortho*-xylene molecules diffusing in SSZ-33 zeolite. Diffusion in the 12-MR channel (parallel to [001]).

5.4. Diffusion in SSZ-33 (CON)

Diffusion results previously obtained in SSZ-33 zeolite [4] and the values of the present simulations are included in Table 5. Both NU-87 and SSZ-33 have connected systems of 12 and 10 MR in their structures, although the latter has a channel structure whereas the former has a channel (10 MR) plus cavities (12 MR) system. It is seen from the values (Table 5) that SSZ-33 allows a better diffusivity of *ortho*-xylene (Fig. 12) and *para*-xylene (Fig. 13) than NU-87. The selectivity for *para*-xylene diffusion obtained by dividing the respective diffusion coefficients in *para*- and *ortho*-xylene gives a larger value (5.8) in NU-87 than in SSZ-33 (3.2 and 2.3 depending on molecular loading). It is also observed when comparing the results in Figs. 12 and 13 that *ortho*-xylene mainly diffuses through the 12-MR channels, while *para*-xylene diffuses also through the 10-MR channels. In zeolites with 10-MR and 12-MR pores, when diffusion through 12-MR channels dominates, the diffusion coefficients for *ortho*- and *para*-xylene tend to equalize, and when the importance of the 12 MR decreases, a larger selectivity for *para*-xylene diffusion appears. The selectivity to diffuse through the 12-MR system can be estimated from the ratio of the *para*- and *ortho*-xylene diffusion coefficients from Table 5, which for β zeolite is 2.3, which is smaller than that for NU-87 (5.8), and similar to that for SSZ-33 (2.3). The diffusivity of 1,2,4-trimethylbenzene (Fig. 14) is, as in all the other cases, lower than that of *ortho*-xylene and the diffusion coefficient 2.53 (from Table 5) is larger than in NU-87 and ZSM-5 zeolites due to the wider channels of SSZ-33, and smaller than that in β where a larger and tridirectional 12-MR channel system is present.

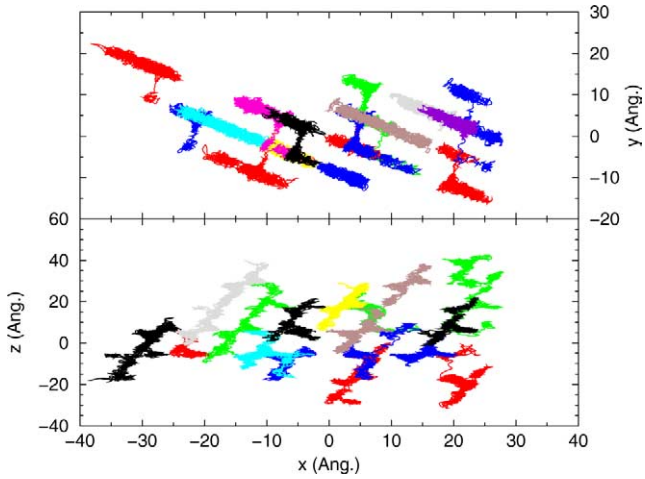

Fig. 13. Trajectories followed by 16 *para*-xylene molecules diffusing in SSZ-33 zeolite. Diffusion in both channel systems is observed: 12-MR (parallel to [001]) and 10-MR channels (parallel to [110]).

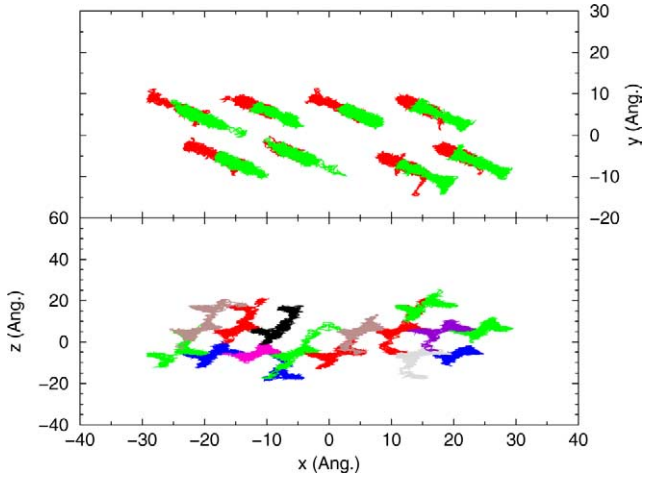

Fig. 14. Trajectories followed by 16 1,2,4-trimethylbenzene molecules diffusing in SSZ-33 zeolite. Diffusion in the 12-MR channel (parallel to [001]) is observed.

From all the above diffusion results, we predict that the catalytic behavior of SSZ-33 toward *meta*-xylene isomerization is as follows: SSZ-33 will give a product distribution closer to that of a 12-MR pore zeolite, such as β, than to a 10-MR zeolite, such as ZSM-5. On the other hand, NU-87 should present a behavior closer to that of a 10-MR zeolite, which will be somewhat limited due to the long residence time of products within the 12-MR cavities that will tend to neutralize the shape-selectivity effects achieved by the diffusion through the 10-MR channels of this structure.

6. Catalytic experiments

6.1. Xylene isomerization-disproportionation

The isomerization and disproportionation of *meta*-xylene have been proposed as a test reaction which allows us to differentiate between 10- and 12-MR pore zeolites, while indicating if there are lobes, cages, or crossing channels [29–36]. This is because during the isomerization of *meta*-xylene, both *para*- and *ortho*-xylenes are formed and, at low levels of conversion, 10-MR pore zeolites give higher *para*/*ortho* ratios (p/o) than 12-MR zeolites. This is rationalized in terms of differences in the diffusion of both isomers through the narrower channels of the 10-MR zeolites. Moreover, the disproportionation of xylenes to give trimethylbenzenes and toluene is a bimolecular reaction, which involves a much bulkier reaction transition state than the monomolecular isomerization process. It is clear that the ratio of isomerization to disproportionation (i/d) will give an indication of the presence of lobes, cavities, or crossing channels where the available space will be large enough to allow the bimolecular reaction to occur.

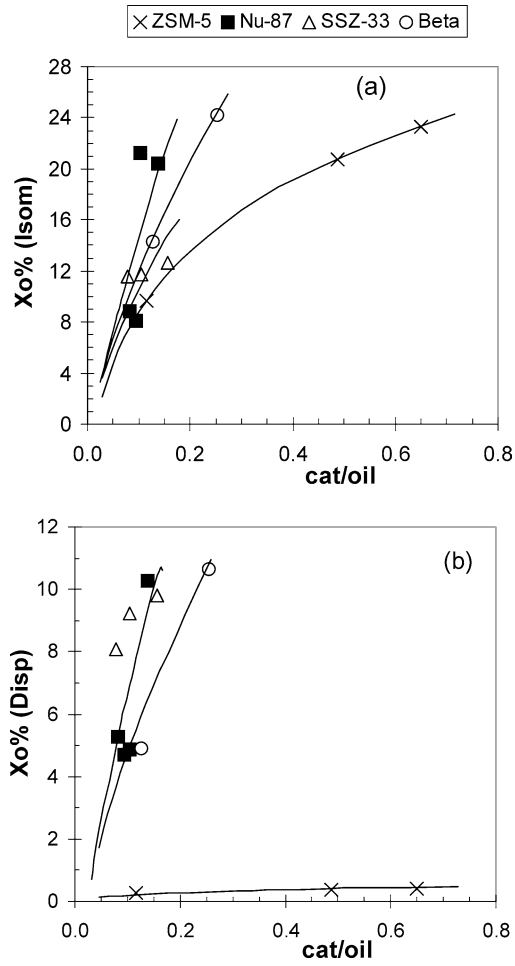

Fig. 15. Initial conversion in the isomerization (a) and disproportionation (b) of *m*-xylene at 623 K and 0.2 atm partial pressure, over ZSM-5, NU-87, SSZ-33, and β versus cat./oil (g of catalyst.h/mol *m*-xylene in feed).

Fig. 15 shows the activity for *meta*-xylene isomerization (a) and disproportionation (b) with ZSM-5, NU-87, SSZ-33, and β zeolites. The activities for all the samples are very similar in the isomerization process (Fig. 15a), whereas significant differences are found especially for the disproportionation process in ZSM-5, where we obtain very low

Table 6
para/*ortho* ratio, isomerization/disproportionation ratio, and distribution of trimethylbenzenes at low conversions of *m*-xylene on different zeolites

Zeolite	X_0 (mol%)	p/o	i/d	Trimethylbenzene (% normalized)			1,2,3/1,3,5 ratio
				1,3,5	1,2,4	1,2,3	
ZSM-5	10.0	2.3	34.3	–	100	–	–
	21.1	2.1	55.0	–	100	–	–
NU-87	26.9	1.3	3.4	2.4	92.5	5.1	2.2
	30.7	1.3	2.4	1.6	93.3	5.1	3.1
SSZ-33	19.6	1.2	1.4	24.6	66.5	8.9	0.36
	22.5	1.2	1.3	24.5	66.9	8.5	0.35
β	19.2	1.1	2.9	26.4	65.8	7.9	0.30
	34.8	1.1	2.3	27.3	64.4	8.3	0.30
Equilibrium (623 K)		1.0		24.0	68.0	8.0	0.33

values. This difference in activity cannot be explained based in the framework Si/Al (Table 4). We consider that the structure of the zeolites determines significant differences in the activity and selectivity. The bigger or smaller difficulty in diffusing the molecules reactants to the active sites, and the same for the molecules produces, justifies the results obtained. In this way in Fig. 15a we represent the activity of the zeolites in the isomerization part of *meta*-xylene transformation, it is perceived that the isomerization activity is practically the same for the four samples at reduced conversion levels. While the difficulties in diffusion and formation of the trimethylbenzenes determine big differences among the activities of disproportionation of ZSM-5 samples, Fig. 15b, as well as significant differences of the selectivities of the trimethylbenzenes formed.

Indeed, although the amount of the stronger Brönsted acid sites required to perform *meta*-xylene isomerization and disproportionation corresponds to those retaining pyridine at 623 K, the desorption temperature [57,58] is larger in NU-87. The initial activity in disproportionation is larger for the β sample, with the amount of Brönsted acid sites lower; again the differences in the structure of the zeolites determine significant differences in the activity.

With respect to product selectivity, NU-87 shows a *para*/*ortho* ratio that is in the expected range for 12-MR zeolites (Table 6). While the molecular dynamics calculations (Table 5) give a p/o diffusivity for NU-87 which is closer to ZSM-5 than to β, the trajectories followed by *para*- and *ortho*-xylene (Figs. 2, 4) clearly show that the residence time of those molecules in the 12-MR cavities of NU-87 will be much larger than in the crossing point of the two channels of ZSM-5 (Figs. 9, 10). It follows that a potential enrichment of *p*-xylene due to diffusional effects in the 10-MR channels of NU-87 will be almost completely neutralized in the 12-MR cavities, and consequently the observed p/o ratio in NU-87 is only slightly larger than in β zeolite. In a similar way, the predominant effect of the 12-MR channels in SSZ-33 (Figs. 12, 13) gives a p/o ratio closer to β than to ZSM-5.

With respect to the xylene i/d ratio, small but significant differences exist. At the same level of total conversion NU-87 always gives an i/d ratio higher than SSZ-33 or β zeolites and smaller than ZSM-5, due to the presence of large cavities in the former zeolite in which there is time and space for *m*-xylene to react, thus increasing disproportionation. It should be taken into account that the results are not masked by the reaction at the external surface since the crystallite size has no significant affect in 12-MR cavities [59]. The molecular dynamics calculations give the trajectories followed by 1,2,4-TMB molecules diffusing in this zeolite (Fig. 3). Intercage migration does appear but only as rare events. Diffusivity is mainly intracavity and this happens with motions going from one side to the other in the cavity, although the number of intracage motions is less frequent than with *ortho*-xylene; a similar situation appears in ZSM-5 zeolite (Fig. 11). The zeolites β (Fig. 8) and SSZ-3 (Fig. 14) show intercage and intracage migration lines similar to *ortho*-xylene diffusion.

An additional selectivity parameter that can be highly informative for the presence of internal cages, lobes, or channel crossing is the distribution of the trimethylbenzene products formed by disproportionation of *meta*-xylene. Indeed, this reaction occurs through the formation of three possible 1,1-diphenylmethane-type transition states [29,37–40] leading to the 1,2,4-, 1,3,5-, and 1,2,3-TMB isomers (Fig. 16). None of the three transition-state complexes can be easily accommodated in the pores of the 10-MR zeolites [34], and when small amounts of disproportionation occur, the less impeded complex that leads to the formation of 1,2,4-TMB should be favored. In Table 6, the distribution of the trimethylbenzenes obtained with zeolite NU-87, at differents levels of *meta*-xylene conversion, is compared with that obtained with ZSM-5, SSZ-33, and β zeolites. It can be seen there that 1,2,4-TMB is initially formed with NU-87 in amounts larger than on SSZ-33 or β zeolite and above the thermodynamic equilibrium, while 1,3,5- and 1,2,3-TMB were formed in lower amounts than those predicted by the thermodynamic equilibrium. The analysis of these results indicates that the less bulky bimolecular transition state (1,2,4-TMB) is clearly favored in the case of NU-87.

The ratio of the initial selectivities for 1,2,3- to 1,3,5-TMB obtained at low levels of disproportionation seems to reflect the shape of the pores. In lobate pores (FAU or L zeolites) the ratio is lower than in zeolites in which the configuration of the side pockets and side channels does not create regular lobes (OFF, MOR, Omega) [34]. In a straight pore with side pockets at regular distances the ratio of 1,2,3-/1,3,5-TMB is initially high, while for 12-MR zeolites consisting of alternating cages or lobes separated by a 12 MR, this ratio is much lower. The ratio of those trimethylbenzene isomers for zeolite NU-87 (Table 6) is higher than for SSZ-33 or β zeolites, indicating that the reactants see smaller void spaces in the NU-87 than in SSZ-33 or β. It

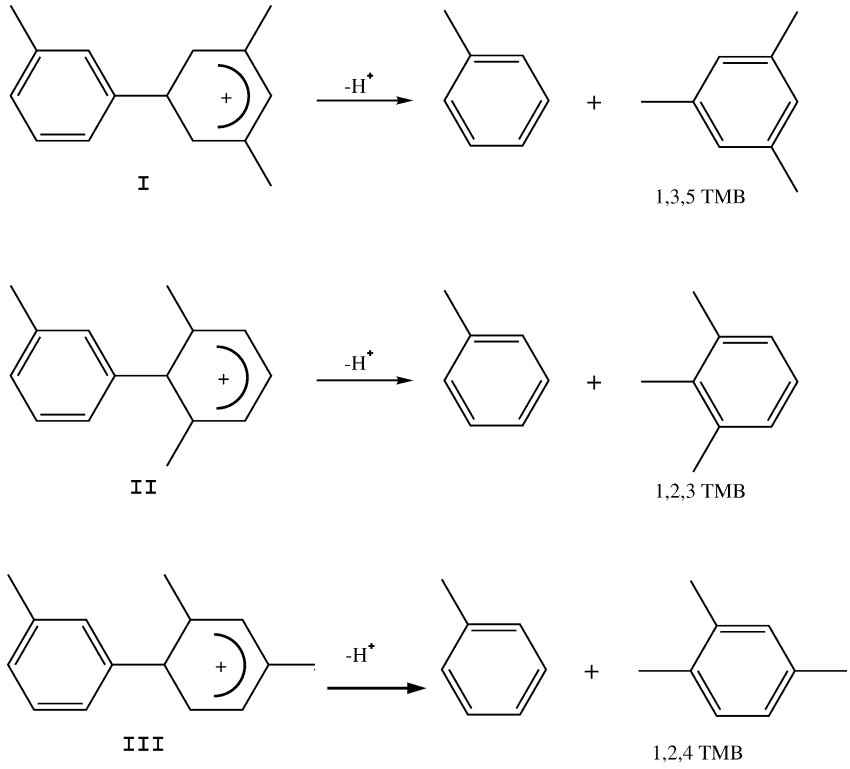

Fig. 16. Possible transition-state complexes for the disproportionation of *meta*-xylene.

should be taken into account that the results are not masked by the reaction at the external surface since the crystallite size of the samples is very similar for ZSM-5, NU-87, and β, and, in any case, is larger for SSZ-33 than for NU-87 (Table 4).

6.2. Toluene alkylation

The alkylation of toluene with alkenes or alcohols are reactions of commercial interest for producing alkyl aromatics such as xylenes, ethyltoluenes and cymenes [41–44]. In view of this, over the past few years, important work has been done to develop heterogeneous systems for this process. In particular, zeolite-type solid acids were reported to produce alkylbenzenes from aromatics and light olefins or alcohols [45–48].

The alkylation of toluene with methanol, ethanol, or propanol can be considered as an electrophilic substitution on the aromatic ring. Alkylation reactions catalyzed by acidic zeolites are commonly considered to proceed via a carbenium ion-type mechanism [46]. When an alcohol is used as an alkylating agent, the isopropylation or ethylation reaction is proposed to take place by protonation of the alcohol on the acid sites of the zeolite, and reaction with toluene producing monoalkylated or polyalkylated aromatics, or reacting with another propanol or ethanol molecule producing C_3^+ products.

It is currently accepted that toluene ring alkylation with methanol proceeds via chemisorption of methanol on the acid sites, followed by formation of surface-active species such as methoxy groups or methoxonium ions [49], which can further react with weakly adsorbed toluene. On the other hand, it is known that dimethylether (DME) is always present, and there are indications that DME can be associated with the alkylation process.

By performing the alkylation of toluene with alcohols of different carbon numbers, we progressively increase the size of the products formed from dimethylbenzenes to ethyltoluenes and to propyltoluene isomers. Table 7 presents conversion and selectivity results for the alkylation of toluene with methanol, ethanol, and propanol over ZSM-5, NU-87, SSZ-33, and β zeolites. In the case of toluene methylation, the main products are xylenes, followed by trimethylbenzenes and other alkylaromatics of high molecular weight in substantially lower amounts. In the case of toluene ethylation, the main products are ethyltoluenes, followed by diethyltoluenes and other alkylaromatics of high molecular weight, especially in β. Finally, the main products in the propylation of toluene are cymenes (isopropyltoluenes), together with benzene, cumene, xylenes, and other alkylaromatics in low concentrations. *n*-Propyltoluenes are also produced via secondary transalkylation of cymenes with toluene [50].

Fig. 17 shows the activity for the toluene reaction with ethanol (a) and isopropanol (b) with ZSM-5, NU-87, SSZ-33, and β zeolites. The activity of the samples shows significant differences especially for the process in ZSM-5, the one in which we obtain very low values. This difference in

Table 7
Conversion and product distribution in toluene alkylation with methanol, ethanol, and isopropanol over ZSM-5, NU-87, SSZ-33 and β samples

Sample	Methanol				Ethanol				Isopropanol			
	ZSM-5	NU-87	SSZ-33	β	ZSM-5	NU-87	SSZ-33	β	ZSM-5	NU-87	SSZ-33	β
Weight catalysts (mg)	203.7	25.5	50.6	51.5	190.9	25.5	25.4	39.3	199.9	25.5	25.4	39.3
WHSV (min^{-1})	1.2	9.6	6.2	17.3	2.2	9.2	13.5	43.6	2.1	9.2	11.8	21.8
Toluene conversion (mol%)[a]	3.1	2.7	6.7	6.7	4.4	9.4	7.6	6.1	4.4	11.2	7.7	10.3
Alcohol conversion (mol%)[a]	100	100	94.8	100	95.8	84.4	60.5	71.2	100	99.4	88.1	99.4
Alcohol yield in products (%)												
Olefins and oligomers	87.0	89.2	57.4	73.6	77.4	39.2	24.5	38.9	79.4	53.3	60.2	56.0
Aromatics	13.0	10.8	37.4	26.4	18.4	45.1	36.0	32.2	20.6	46.1	27.9	43.4
No reaction	0.0	0.0	5.2	0.0	4.2	15.6	39.5	28.8	0.0	0.6	11.9	0.6
Aromatic product distribution (%)[b]												
Benzene	0	9.7	3.5	9.9	0.6	0.1	1.8	1.1	3.6	0.1	1.8	0.0
Ethylbenzene	–	–	–	–	3.3	1.8	3.4	0.0	1.5	0	0.3	0.7
Xylenes	93.6	77.4	77.6	78.5	3.9	1.9	5.6	0.6	5.1	1.8	4.2	1.4
Cumene	–	–	–	–	–	–	–	–	0.0	1.8	1.6	2.0
Ethyltoluenes	–	–	–	–	89.0	75.8	68.3	66.4	–	–	–	–
Cymenes	–	–	–	–	–	–	–	–	40.4	93.7	82.9	89.1
Propyltoluenes	–	–	–	–	–	–	–	–	46.2	0.9	1.5	1.4
Trimethylbenzenes	6.4	9.1	13.1	11.6	–	–	–	–	–	–	–	–
Diethyltoluenes	–	–	–	–	2.8	18.0	17.1	19.6	–	–	–	–
Dipropyltoluenes	–	–	–	–	–	–	–	–	3.2	1.9	4.7	5.5
Others aromatics	0	3.8	5.7	0	0.5	2.5	3.7	12.2	0	0	2.9	0
Normalized distribution (%)[c]	Xylenes				Ethyltoluenes				Cymenes			
Para	59.3	26.1	30.9	29.4	70.3	22.5	26.7	26.8	92.1	38.9	39.3	28.5
Meta	21.5	22.8	28.7	22.1	26.3	55.6	44.5	33.8	6.9	54.9	51.2	60.1
Ortho	19.2	51.1	40.4	48.5	3.5	21.9	28.8	39.4	1.0	6.1	9.4	11.4

Reaction conditions: Toluene to alcohol molar ratio, 4; temperature, 573 K.
[a] Toluene and alcohol conversions obtained at 30 s time on stream.
[b] Toluene free.
[c] Calculated thermodynamic equilibria at 573 K, give a *para*/*meta*/*ortho* distribution of xylenes, 24.1/53.4/22.5; ethyltoluenes, 34.1/50.0/15.9; and of cymenes, 22.6/63.2/14.2.

activity cannot be explained based on the framework Si/Al and number and strength of acid sites within the zeolites shown in Table 4. The structure of the zeolites determines significant differences in the activity and selectivity. The bigger or smaller difficulty in diffusing the molecules produces justifies the results obtained. In this way in Fig. 17a, it is perceived that the toluene activity is practically the same for the NU-87 and SSZ-33 samples and yet, the selectivity to ethyltoluenes obtained during toluene alkylation with ethanol is higher with NU-87 than with SSZ-33 and β (Table 7). The difficulties in diffusion and formation of the ethyltoluenes determine the differences among the activities of the ZSM-5 samples, as well as significant differences of the selectivities of the diethyltoluenes formed.

On the other hand, as seen in Fig. 17b the activity in toluene alkylation with isopropanol is practically the same for the NU-87 and SSZ-33 samples. But cymenes prevail among the products obtained, giving values higher than 90% for the selectivity of aromatics with NU-87 zeolites. Again the difficulties in diffusion and formation of the cymenes determine the differences among the activity of ZSM-5 sample, as well as significant differences of the selectivity of the *n*-propyltoluenes formed.

The selectivity differences observed for xylenes, ethyltoluenes, and diethyltoluenes on NU-87 and the other zeolites can be related to channel structure and differences in the kinetic diameters of the aromatic molecules produced. In this way, the selectivity to monoalkylated products, i.e., xylenes and ethyltoluenes, is larger with ZSM-5 than with NU-87 due to larger pore restrictions existing in the former for formation and diffusion of the dialkylated and trialkylated products. However, this selectivity is larger with NU-87 than with SSZ-33 or β zeolite due to the larger diffusional limitations existing in the 10-MR channel of NU-87 for dialkylated and trialkylated products.

Meanwhile, in the alkylation of toluene with isopropanol, the increment in size of the alkylaromatics formed creates differences in the diffusion of cymenes within the zeolites structures studied here. In this way, the selectivity to monoalkylated products, i.e., cymenes, is larger with NU-87 than with SSZ-33 and β due to the larger pore restrictions in the former for formation and diffusion of the dialkylated and trialkylated products.

6.2.1. *para*-Selectivity

Fig. 18 depicts the *para*/*ortho* ratio (p/o) of the isomers produced in alkylation reactions. If one takes into account

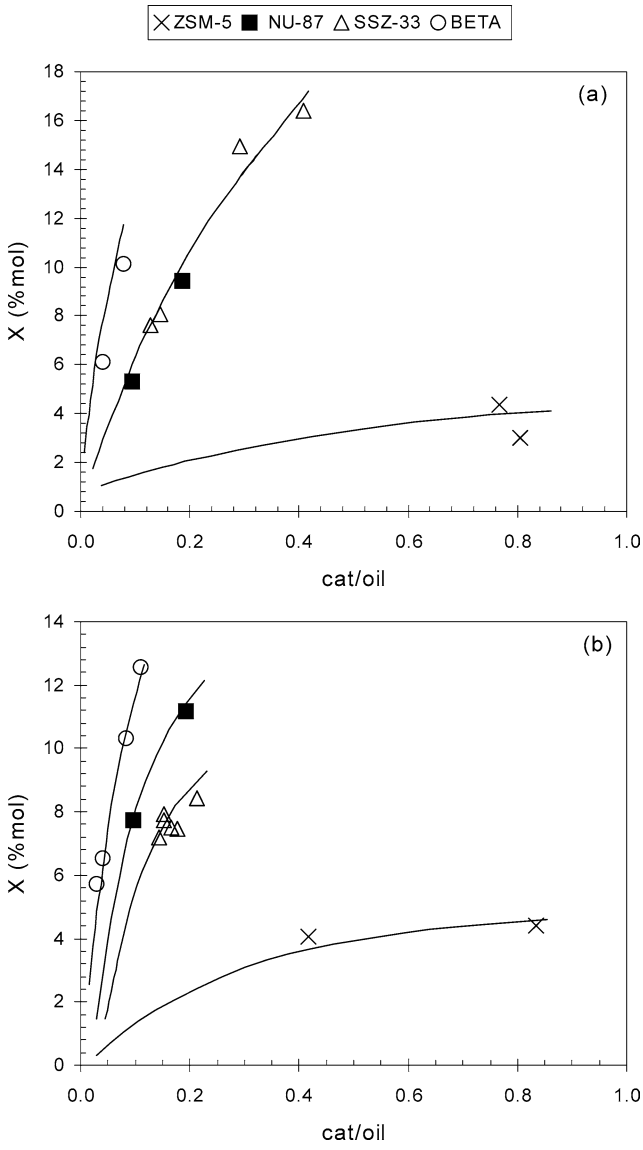

Fig. 17. Conversion versus cat./oil in the alkylation of toluene with ethanol (a) and isopropanol (b) at 573 K over zeolites ZSM-5, NU-87, SSZ-33, and β versus cat./oil (g of catalyst.h/mol m-xylene in feed).

that the molecular size of the alkylated products increases in the order xylene < ethyltoluene < cymene, we can predict that the experimental *para* to *ortho* ratio should increase when increasing the molecular size of the products (p/o-xylene < p/o-ethyltoluene < p/o-cymene). This indeed occurs in ZSM-5, for which a higher *para* to *ortho* ratio is obtained in all cases.

While the isomer distribution in xylenes gives a p/o ratio in NU-87 close to zeolites SSZ-33 or β, the isomer distribution in ethyltoluenes, which have a slightly larger size than dimethylbenzenes, gives a p/o ratio in NU-87 significantly higher than zeolites SSZ-33 or β because of the larger restrictions in diffusion for *ortho*-ethyltoluene. As it could be expected, the diffusion of the *ortho*-cymene is relatively slower in NU-87 than in SSZ-33 or β zeolite, showing again

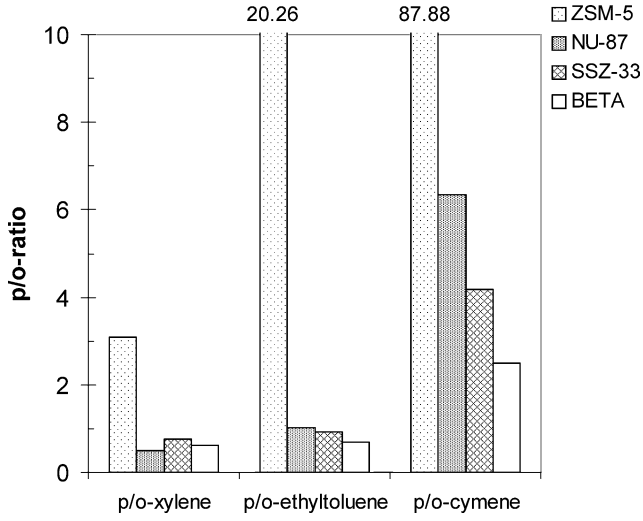

Fig. 18. *para*/*ortho* ratio of xylene, ethyltoluene, and cymene isomers, in the alkylation process of toluene with methanol, ethanol, and isopropanol, respectively, at 573 K, over zeolites ZSM-5, NU-87, SSZ-33, and β.

that difference in pore dimensions and topology can significantly affect selectivity.

6.3. Iso- and n-propyl alkylaromatics

Despite the fact that there are numerous studies in the open literature on the propylation of toluene over large and medium pore zeolites, the mechanism of the formation of n-propyl aromatics, the main undesired product, has not been elucidated until recently [50,51]. Initially, n-propyl aromatics were supposed to be generated via monomolecular isomerization of the isopropyl isomers formed in the first alkylation step [42]. However, it has now been shown [52–54] that the formation of n-propyl isomers is the result of a transalkylation reaction of cymene with toluene. Ivanova et al. [55], studying the alkylation of benzene with labeled propylene on H-ZSM-11 by in situ ^{13}C MAS NMR, came to the conclusion that n-propylbenzene formation takes place via an intermolecular reaction between cumene and benzene. When only isopropyltoluenes were contacted with the zeolites, no n-propyl isomers were detected. Wichterlová and Cejka [51] have found that the formation of n-propyltoluenes is strongly dependent on the dimensions and architecture of the channels of the molecular sieve.

For ZSM-5 a low ratio of cymenes to n-propyltoluenes is obtained (Table 7), because the channel intersections in three-dimensional structure of this zeolite, where the perpendicularity of the intersecting channels favors the n-propyltoluene formation.

For NU-87, SSZ-33, and β zeolites, the former produces, specially at low conversions, higher ratios of cymenes to n-propyltoluenes. This is in agreement with the more favorable environment of SSZ-33 and β for bimolecular reactions of bulky reactants such as those required for n-propylbenzene formation.

7. Conclusions

Diffusion studies of *ortho*- and *para*-xylene and 1,2,4-trimethylbenzene in NU-87 predict that while the three molecules can diffuse from one large cavity to another through the 10-MR channels, the diffusion coefficients should be lower than in a bidimensional 10-MR pore zeolite such as ZSM-5. This means that during *meta*-xylene isomerization, one can expect that reactants and products formed by methyl-shift isomerization or alkyl-shift transalkylation will spend a considerable time within the NU-87 cavity before intercavity migration occurs. This drives the mixture toward thermodynamic equilibrium, neutralizing diffusion shape-selectivity effects that will tend to enrich the gaseous stream with *para*-xylene. Furthermore, trimethylbenzenes formed tend to equilibrate, but only the smaller isomer, i.e., 1,2,4-trimethylbenzene, fits in the NU-87 cavity and has a small chance to diffuse. This is responsible for the high selectivity to 1,2,4-trimethylbenzene, and a fast deactivation by pore blocking.

A 12-MR channel system is much more suitable for diffusion than a system of 12-MR cavities interconnected through 10-MR channels, and this is not only because of the 10-MR intercage connection between cavities but also due to the fact that changing the diffusion direction when entering and leaving the cavities causes a substantial drop in the diffusivity. Channels offer a less restricted trajectory system than cavities interconnected perpendicularly.

With respect to the *m*-xylene i/d ratio NU-87 always gives a ratio higher than SSZ-33 or β zeolites and smaller than ZSM-5, due to the presence of large cavities in which there is time for *m*-xylene to react, thus increasing disproportionation. The ratio of 1,2,3-/1,3,5-TMB isomers for NU-87 is higher than for SSZ-33 or β zeolites, indicating that the reactants see smaller void spaces in the NU-87 than in SSZ-33 or β.

The selectivity differences observed for xylenes, ethyltoluenes, and diethyltoluenes produced by toluene alkylation with methanol, ethanol, propanol and isopropanol are related to channel structure and to differences in the kinetic diameter of the aromatic molecules produced. The selectivity to monoalkylated products is larger with ZSM-5 than with NU-87 due to larger pore restrictions existing in the former for formation and diffusion of the dialkylated and trialkylated products. However, this selectivity is larger with NU-87 than with SSZ-33 or β zeolite due to the larger diffusional limitations existing in the 10-MR channel of NU-87 for dialkylated and trialkylated products.

Meanwhile, in the alkylation of toluene with isopropanol, while the isomer distribution in xylenes gives a p/o ratio in NU-87 close to zeolites SSZ-33 or β, the isomer distribution in ethyltoluenes, which have a slightly larger size than dimethylbenzenes, gives a p/o ratio in NU-87 significantly higher than zeolites SSZ-33 or β because of the larger restrictions in diffusion for *ortho*-ethyltoluene. As expected, the diffusion of the *ortho*-cymene is relatively slower in NU-87 than in SSZ-33 or β zeolite, showing again that differences in pore dimensions and topology can significantly affect selectivity.

In the propylation of toluene, the formation of *n*-propyl isomers is strongly dependent on dimensions and architecture of the channels of the molecular sieve. In the case of ZSM-5 a low ratio of cymenes to *n*-propyltoluenes is obtained because the channel intersects in a three-dimensional structure of this zeolite, where the perpendicularity of the intersecting channels favors the *n*-propyltoluene formation. In the case of NU-87, SSZ-33, and β zeolites, the former produces, specially at low conversions, higher ratios of cymenes to *n*-propyltoluenes. This is in agreement with the more favorable environment of SSZ-33 and β for bimolecular reactions of bulky reactants.

Acknowledgments

We thank Centro de Cálculo de la Universidad Politécnica de València for the use of their computational facilities. Ministerio de Ciencia y Tecnologia of Spain is acknowledged for providing funds through project MAT2003-07769-C02-01.

References

[1] A. Corma, V. Gonzalez-Alfaro, A.V. Orchilles, J. Catal. 216 (2003) 298.
[2] A. Corma, A.V. Orchilles, Micropor. Mesopor. Mater. 35 (2000) 21.
[3] E.G. Derouane, Z. Gabelica, J. Catal. 65 (1980) 486.
[4] G. Sastre, N. Raj, C.R.A. Catlow, R. Roque-Malherbe, A. Corma, J. Phys. Chem. B 102 (1998) 3198.
[5] M.E. Leonowicz, J.A. Lawton, S.L. Lawton, M.K. Rubin, Science 264 (1994) 1910.
[6] (a) S. Laforge, D. Martin, M. Guisnet, Micropor. Mesopor. Mater. 67 (2004) 235;
(b) A. Corma, C. Corell, F.J. Llopis, A. Martinez, J. Perez-Pariente, Appl. Catal. A 115 (1994) 121.
[7] G. Bellusi, G. Perego, M.G. Clerici, A. Giusti, EPA 293032 (1998).
[8] A. Corma, V. Fornes, S.B. Pergher, T.L.M. Maesen, J.G. Buglass, Nature 396 (1998) 353.
[9] (a) B. Onida, L. Borello, B. Bonelli, F. Geobaldo, E. Garrone, J. Catal. 214 (2003) 191;
(b) C. Baleizao, B. Gigante, H. Garcia, A. Corma, J. Catal. 215 (2003) 199.
[10] H.D. Shannon, J.L. Casci, P.A. Cox, S.J. Andrews, Nature 353 (1991) 417.
[11] A. Corma, E. Benazzi, H. Cauffriez, M.J. Diaz-Cabañas, M.S. Grande-Casas, M.A. Camblor, G. Mabilon, EP 855369 (1999).
[12] (a) J.L.Casci, EP 377291 (1989);
(b) J.L. Casci, I.J.S. Lake, T.R. Maberly, US patent 5041402 (1991).
[13] T.R. Forester, W. Smith, J. Mol. Graphics 14 (1996) 136.
[14] L. Verlet, Phys. Rev. 159 (1967) 98.
[15] D.F. Shannon, Math. Comp. 24 (1970) 647.
[16] J.D. Gale, J. Chem. Soc., Faraday Trans. 93 (1997) 629.
[17] P. Demontis, E.S. Fois, G.B. Suffriti, S. Quartieri, J. Phys. Chem. 94 (1990) 4329.
[18] S. Yashonath, J.M. Thomas, A.K. Nowak, A.K. Cheetham, Nature 331 (1988) 601.
[19] G. Schrimpf, M. Schlenkrich, J. Brickmann, P. Bopp, J. Phys. Chem. 96 (1992) 7404.

[20] M.P. Allen, D. Tildesley, Molecular Simulation of Liquids, Oxford Univ. Press, London, 1980.
[21] C.R.A. Catlow, C.M. Freeman, B. Vessal, S.M. Tomlinson, M. Leslie, J. Chem. Soc., Faraday Trans. 87 (1991) 1947.
[22] T. Oie, T.M. Maggiora, R.E. Christoffersen, D.J. Duchamp, Int. J. Quantum Chem., Quantum Biol. Symp. 8 (1981) 1.
[23] S.M. Auerbach, N.J. Henson, A.K. Cheetham, H.I. Metiu, J. Phys. Chem. 99 (1995) 10600.
[24] Ch. Baerlocher, W.M. Meier, D.H. Olson, Atlas of Zeolite Framework Types, fifth ed., Elsevier, 2001, Also in URL, http://www.iza-structure.org.
[25] (a) J.B. Higgins, R.B. LaPierre, J.L. Schlenker, A.C. Rohrman, J.D. Wood, G.T. Kerr, W.J. Rohrbaugh, Zeolites 8 (1988) 446;
(b) J.M. Newsam, M.M.J. Treacy, W.T. Koetsier, C.B. Gruyter, Proc. Roy. Soc. London A 420 (1988) 375.
[26] H. van Koningsveld, H. van Bekkum, J.C. Jansen, Acta Crystallogr. B 43 (1987) 127.
[27] R.F. Lobo, M.E. Davis, J. Am. Chem. Soc. 117 (1995) 3764.
[28] R.F. Lobo, M. Pan, I. Chan, H.X. Li, R.C. Medrud, S.I. Zones, P.A. Crozier, M.E. Davis, Science 262 (1993) 1453.
[29] M. Guisnet, N.S. Gnep, S. Morin, Micropor. Mesopor. Mater. 35–36 (2000) 47.
[30] P. Meriaudeau, V.A. Tuan, V.T. Nghiem, F. Lefebvre, V.T. Ha, J. Catal. 185 (1999) 378.
[31] P. Wu, T. Komatsu, T. Yashima, Micropor. Mesopor. Mater. 22 (1998) 343.
[32] A. Corma, Micropor. Mesopor. Mater. 21 (1998) 487.
[33] J.A. Martens, J. Pérez-Pariente, E. Sastre, A. Corma, P.A. Jacobs, Appl. Catal. 45 (1988) 85.
[34] L.B. Young, S.A. Butter, W.W. Kaeding, J. Catal. 76 (1982) 418.
[35] D.H. Olson, W.O. Haag, ACS Symp. Ser. 248 (1984) 275.
[36] H. Du, D.H. Olson, J. Phys. Chem. B 106 (2002) 395.
[37] A. Corma, F.J. LLopis, J.B. Montón, J. Catal. 140 (1993) 384.
[38] Y. Xiong, P.G. Rodewald, C.D. Chang, J. Am. Chem. Soc. 117 (1995) 9427.
[39] D.S. Santilli, J. Catal. 99 (1986) 327.
[40] B. Adair, C.Y. Chen, K.T. Wan, M.E. Davis, Micropor. Mesopor. Mater. 7 (1996) 261.
[41] W.W. Kaeding, C. Chu, L.B. Young, B. Weinstein, S.A. Butter, J. Catal. 67 (1981) 159.
[42] J. Cejka, B. Wichterlova, Catal. Rev.-Sci. Eng. 44 (2002) 375.
[43] G. Mirth, J.A. Lercher, J. Catal. 147 (1994) 199.
[44] A.B. Halgeri, J. Das, Appl. Catal. A 181 (1999) 347.
[45] G. Bellusi, G. Pazzucini, C. Perego, G. Girotti, G. Terzoni, J. Catal. 157 (1995) 227.
[46] S. Siffert, L. Gaillard, B.L. Su, J. Mol. Catal. A Chem. 153 (2000) 267.
[47] C. Perego, S. Amarilli, R. Millini, G. Bellussi, G. Girotti, G. Terzoni, Micropor. Mater. 6 (1996) 395.
[48] A. Corma, V. Martínez-Soria, E. Schnoeveld, J. Catal. 192 (2000) 163.
[49] I.I. Ivanova, A. Corma, Stud. Surf. Sci. Catal. 97 (1995) 27.
[50] B. Wichterlová, J. Cejka, N. Zilková, Micropor. Mater. 6 (1996) 405.
[51] B. Wichterlová, J. Cejka, J. Catal. 136 (1994) 523.
[52] I.I. Ivanova, D. Brunel, J.B. Nagy, G. Daelen, E.G. Derouane, Stud. Surf. Sci. Catal. 78 (1993) 587.
[53] I.I. Ivanova, E.G. Derouane, Stud. Surf. Sci. Catal. 85 (1994) 361.
[54] I.I. Ivanova, D. Brunel, J.B. Nagy, E.G. Derouane, J. Mol. Catal. A 95 (1995) 243.
[55] I.I. Ivanova, F. Fajula, in: M.M.J. Treacy, B.K. Marcus, M.E. Bisher, J.B. Higgins (Eds.), Proc. 12th Int. Zeolite Conf., 1998, p. 2273.
[56] C.A. Emeis, J. Catal. 141 (1993) 347.
[57] A. Corma, V. Fornés, J. Pérez-Pariente, E. Sastre, J.A. Martens, P.A. Jacobs, ACS Symp. Ser. 368 (1988) 555.
[58] D. Meloni, S. Laforge, D. Martin, M. Guisnet, E. Rombi, V. Solinas, Appl. Catal. A 215 (2001) 55.
[59] A. Corma, V.I. Costa-Vaya, M.J. Díaz-Cabañas, F.J. Llopis, J. Catal. 207 (2002) 46.